

OPEN ACCESS

Safety of Aged Li-Ion Cells without Lithium Plating – An ARC-EIS Study

To cite this article: Philipp Moosmann *et al* 2025 *J. Electrochem. Soc.* **172** 080516

View the [article online](#) for updates and enhancements.

You may also like

- [Examining the Critical Residual Moisture Threshold of Gr/NMC622-based Li-Ion Batteries](#)
Hans Fenske, Valerie Nastassia Mohni, René Jagau et al.
- [Performance Changes of Lithium-Ion-Batteries due to Electrolyte-Introduced Metal Oxalate Contaminants](#)
Anna Rollin, Ziang Wang, Petr Novák et al.
- [Cycling Aging in Different State of Charge Windows in Lithium-Ion Batteries with Silicon-Dominant Anodes](#)
S. Friedrich, M. Bock and A. Jossen

ECC-Opto-10 Optical Battery Test Cell: Visualize the Processes Inside Your Battery!

EL-CELL®
electrochemical test equipment

✓ **Battery Test Cell for Optical Characterization**

Designed for light microscopy, Raman spectroscopy and XRD.

✓ **Optimized, Low Profile Cell Design (Device Height 21.5 mm)**

Low cell height for high compatibility, fits on standard samples stages.

✓ **High Cycling Stability and Easy Handling**

Dedicated sample holders for different electrode arrangements included!

✓ **Cell Lids with Different Openings and Window Materials Available**



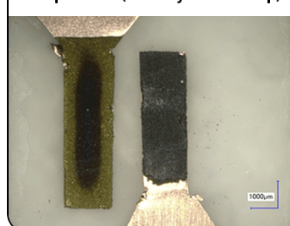
Contact us:

+49 40 79012-734

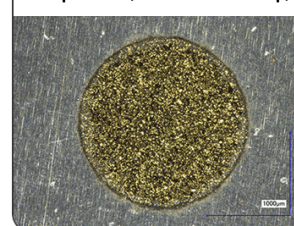
sales@el-cell.com

www.el-cell.com

Sample Test (Side-by-Side Setup)




Sample Test (Face-to-Face Setup)





Safety of Aged Li-Ion Cells without Lithium Plating – An ARC-EIS Study

Philipp Moosmann,^{1,2} Jihed Ayari,^{3,4} Ilona Jipa,² Markus Hölzle,^{1,*} and Thomas Waldmann^{1,3,5,z} 

¹ZSW—Zentrum für Sonnenenergie- und Wasserstoff-Forschung Baden-Württemberg, 89081 Ulm, Germany

²Dr. Ing. h.c. F. Porsche Aktiengesellschaft, 70435 Stuttgart—Zuffenhausen, Germany

³HIU—Helmholtz Institute Ulm for Electrochemical Energy Storage, 89081 Ulm, Germany

⁴Karlsruhe Institute of Technology (KIT), 76021 Karlsruhe, Germany

⁵Ulm University—Institute of Surface Chemistry and Catalysis, 89069 Ulm, Germany

The thermal runaway behavior of commercial high-energy 18650 lithium-ion batteries with Si/graphite anodes and Ni-rich NMC cathodes was investigated by ARC-EIS, accelerating rate calorimetry (ARC) in combination with electrochemical impedance spectroscopy (EIS). The cells were cyclically aged at a rate of 1C and at 45 °C without Li plating. Aging was characterized electrochemically by Arrhenius plots of initial aging rates and differential voltage analysis (DVA). The effects of state of health (SoH) and state of charge (SoC) in ARC experiments were investigated regarding the onset of self-heating temperature T_{SH} , venting temperature T_{vent} , onset of thermal runaway temperature T_{TR} , and mass loss. With the aim of early thermal runaway detection without temperature measurement, an ARC-EIS method is proposed. This approach is based on impedance changes during thermal runaway at different SoH and SoC. A correlation between T_{SH} , indicating significant exothermic reactions, and different impedance values ($Re(Z)$, $\varphi(Z)$, and Nyquist integral) was observed for different SoH and SoC levels.

© 2025 The Author(s). Published on behalf of The Electrochemical Society by IOP Publishing Limited. This is an open access article distributed under the terms of the Creative Commons Attribution 4.0 License (CC BY, <https://creativecommons.org/licenses/by/4.0/>), which permits unrestricted reuse of the work in any medium, provided the original work is properly cited. [DOI: 10.1149/1945-7111/adf5eb]



Manuscript submitted June 16, 2025; revised manuscript received July 18, 2025. Published August 14, 2025.

Lithium-ion batteries (LIBs) are currently the leading battery technology. In 2024, fully commissioned global battery-cell manufacturing capacity was approximately 3.1 terawatt-hours (TWh).¹ For automotive applications, high-energy batteries are of particular interest, including those utilizing nickel-rich layered oxide cathodes and silicon/graphite (Si/C) anodes. Under certain conditions, cells may enter thermal runaway (TR), a phenomenon where the battery uncontrollably releases energy, potentially causing fires or explosions.^{2–4} Understanding the safety behavior of these cells at different SoC and SoH is critical for enhancing their safety and reliability over lifetime.^{2,5}

In recent years significant research has been conducted on Ni-rich NMC||Si/C cells, particularly focusing on how their chemical and physical properties evolve under different operating conditions.^{6–9} Typical aging mechanisms in LIBs include solid electrolyte interphase (SEI) growth^{10–12} and lithium plating,^{11–14} both of which contribute to the loss of lithium inventory (LLI) and significantly impact the safety characteristics of the battery.¹⁵ ARC has proven to be a valuable technique for characterizing the thermal behavior of these batteries, offering insights into the onset of TR and the associated exothermic reactions.^{2,5,16–25} However, while ARC tests provide comprehensive thermal profiles, the combination with EIS can further enrich the understanding of the degradation mechanisms and the early detection of unsafe conditions.¹⁶ EIS, in particular, has emerged as a tool for the early detection of TR by monitoring changes in cell impedance, which are indicative of internal resistance increases due to degradation or abnormal cell behavior.^{16,26} The crosslink between impedance changes and thermal stability at different SoH and SoC levels is related to the changes in SEI formation and decomposition processes at rising temperature.^{16,27} Srinivasan et al. showed in constant power heating tests of 18650 cylindrical LIB cells that the phase shift of the impedance $\varphi(Z)$ at a frequency of 5 Hz can be a robust indicator of impending venting and TR without the need for φ vs temperature calibration, which therefore is a valuable criterion for hazard prevention.²⁶ In continuing work, Srinivasan et al. showed that an increase in anode temperature above 75 °C, induced by a single high-rate ($\geq 3C$)

discharge cycle, permanently changes the cell impedance similarly to 15 months of calendar aging at room temperature (RT) due to loss of lithium ions from the electrolyte and SEI growth.¹⁶ This is reflected in a shift of impedance spectra toward higher values of the real part of the impedance, $Re(Z)$.¹⁶ This leads to the conclusion that the shift in $Re(Z)$ can be used for SEI degradation detection, although the phase shift in a frequency range from 40–100 Hz, which is typically related to SEI processes,^{28,29} tends asymptotically toward zero degree at high temperatures.²⁹

To the best of our knowledge, there is so far no article published where impedance spectra of a large number of cells were measured under quasi-adiabatic conditions and analyzed regarding their safety behavior. This paper aims to systematically evaluate the safety behavior with a focus on the early stages of TR in commercial Ni-rich NMC||Si/C 18650 cylindrical LIB cells across various SoC and SoH levels. The cells were aged at high temperatures to exclude the effects of Li plating. First, the cells are analyzed electrochemically using differential voltage analysis (DVA) and Arrhenius plots of aging rates. Next, ARC is used to assess thermal stability and TR behavior. Finally, a novel EIS-based approach is employed to analyze early-stage failure behavior. By correlating impedance changes with TR events, this research seeks to develop a predictive framework for identifying unsafe operating conditions before they escalate into critical failures.

Experimental

Investigated cells.—The studied commercial Ni-rich NMC||Si/C 18650 cylindrical LIB cells designed for high-energy applications are rated at a nominal discharge capacity of 3.5 Ah at 0.2C. Upon arrival of the cells, each cell was weighed ($47.6 \text{ g} \pm 0.2 \text{ g}$) and the voltage ($3.597 \text{ V} \pm 0.002 \text{ V}$) as well as the internal resistance ($28.0 \text{ m}\Omega \pm 0.2 \text{ m}\Omega$) were determined at a frequency of 1 kHz using a Hioki 3554 battery tester. The standard deviations observed across the measured cell batch (73 cells) are similarly low compared to those of other cell types, indicating suitability for further investigation.³⁰ More information can be found in Flügel et al., who investigated the same cell type (type C).⁷

Cyclic aging procedure.—To investigate cyclic aging, the cells were continuously charged and discharged inside a climate chamber

*Electrochemical Society Member.

^zE-mail: thomas.waldmann@zsw-bw.de

Table I. Overview of aging tests in this study.

SoH/%	SoC/%	Number of cells
100	100	4
100	90	2
100	70	2
100	30	2
90	100	3
80	100	3
70	100	3
70	70	2
70	30	2

(Vötsch) at 45 °C using a 1C CC-CV protocol with a BaSyTec CTS system. To determine the current SoH of the cells at time t , the discharge capacity $Q(t)$ from the latest cycle was referenced to the discharge capacity $Q(t = 0)$ of the first discharge cycle according to Eq. 1. After reaching a target SoH of 90%, 80%, or 70%, the aging was stopped. Subsequently, quasi-stationary open-circuit voltage (qOCV) measurements were conducted at 25 °C following a C/20 rate CC-CV protocol.

$$SoH(t) = \frac{Q(t)}{Q(t = 0)} \cdot 100\% \quad [1]$$

An overview of the tested cells is given in Table I.

In addition to the tests listed in Table I, 16 additional cells were aged (BaSyTec CTS, 1C CC-CV protocol) inside Espec and Vötsch environmental test chambers at eight different temperatures, ranging from −10 °C to 45 °C, with duplicates at each condition.

Impedance test setup.—Impedance measurements were conducted using a Biologic SP150 impedance analyzer with an excitation amplitude of 250 mA. Data was recorded across a frequency range from 100 kHz to 50 mHz, with ten points per decade and three measurements per frequency. Each impedance spectrum was measured in duplicate. All impedance features $x(Z)$ are normalized with respect to their initial values $x_{start}(Z)$ as described in Eq. 2 to enable comparison of cells across different SoH and SoC levels.

$$x(Z)_{norm} = \frac{x(Z)}{x_{start}(Z)} \quad [2]$$

ARC test setup.—All ARC testing was conducted in a THT ARC ES adiabatic battery testing system using the standard heat-wait-see (HWS) protocol. A calibration and subsequent drift check of the ARC system with an empty 18650 size cell housing ensured the correct heating power of the heaters in the ARC device to provide quasi-adiabatic conditions. For both calibration and testing, the same type N thermocouple was used. It was placed at the center of the side surface of the battery. Testing commenced at a start temperature (T_{start}) of 35 °C, with incremental temperature steps of 5 °C and a final temperature (T_{final}) of 350 °C. Each step included a wait time (t_{wait}) of 20 min, with a temperature rate sensitivity threshold of 0.02 °C min^{−1}. The process is schematically illustrated in Fig. 1a. During exothermic mode, the calorimeter followed the cell temperature, leading to quasi-adiabatic conditions.

Following cycling at 45 °C to reach the specified SoH, cells were charged to the designated SoC with respect to their actual capacity at 25 °C. To prepare for testing, twisted wires were soldered to the cell terminals using a four-point connection to ensure accurate impedance measurement. Cells were then insulated with Kapton® tape and fixed to the ARC's top cover using a cell holder covering the cell shell surface. Initial impedance measurements of both cells and the

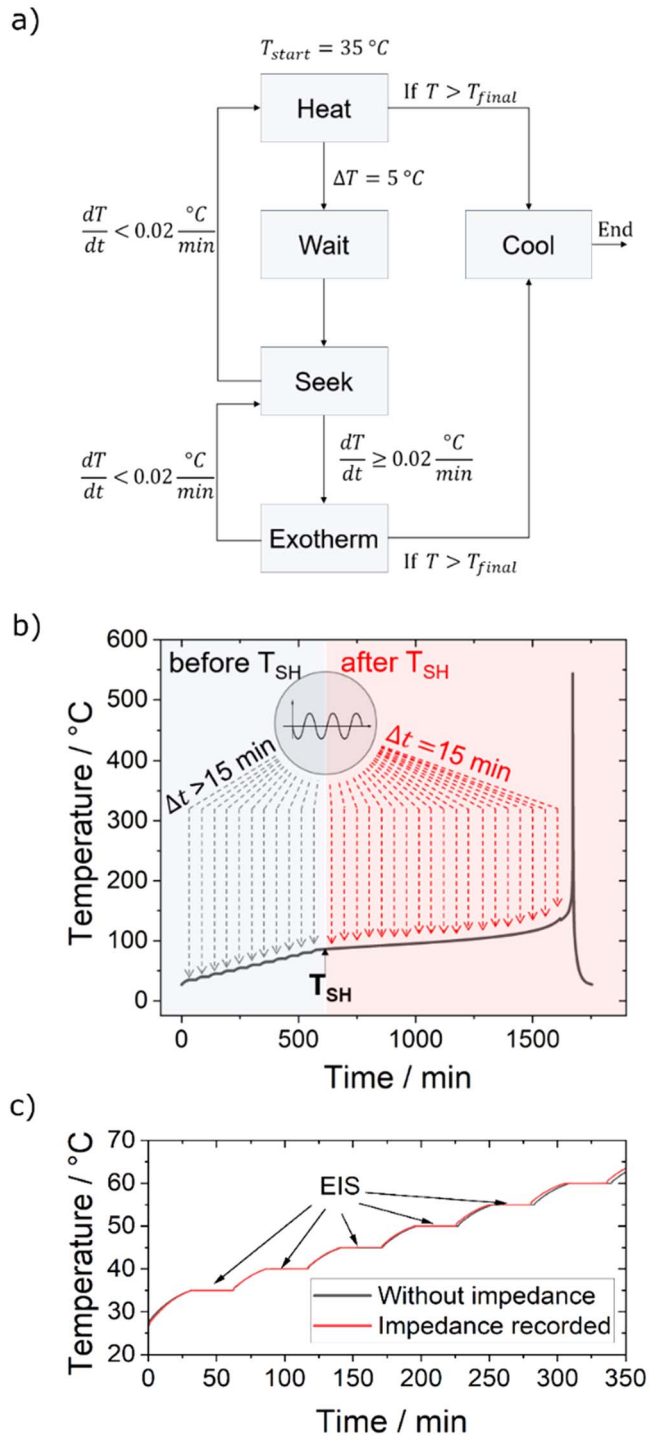


Figure 1. (a) Flowchart of a heat-wait-see measurement adapted from Lei et al.³¹ and (b) schematic representation of an ARC measurement curve with recorded impedance spectra below and above T_{SH} . Impedance measurements do not noticeably influence the cell behaviour during the experiment (c).

test setup were conducted at RT ($\sim 25\text{ °C}$). The ARC test followed the established protocol: Two impedance spectra were recorded during each wait phase, with measurements initiated following a 5 min rest period. Above the onset of self-heating T_{SH} phase, impedance measurements were taken at 15 min intervals (see Fig. 1b). As shown in Fig. 1c, the seek phase is not influenced by the EIS measurements, as heat produced is negligible due to the low excitation current amplitude ($\leq C/10$) applied to all cells.

Results and Discussion

Aging analysis.—Figure 2a presents the qOCV curves across different SoH levels recorded at a rate of C/20. The qOCV curves for aged cells exhibit a steeper slope, indicating increased polarization effects, and show a leftward shift in voltage, reflecting diminished capacity retention. Both effects together reduce the energy content of the cell, which is represented by the area under the curves. The qOCV curves reveal no distinct potential plateau at high SoC (low discharge capacity, left-hand side of the plot). The absence of this shoulder^{17,32,33} does not indicate any Li deposition during cyclic aging at 1C/45 °C, which is consistent with the results of voltage relaxation and GD-OES depth profiling by Flügel et al. for the same cell type for aging at 0.85C/45 °C.⁷

In the DVA curves in Fig. 2b, the first peak that is caused by silicon (S1) during discharge progressively diminishes with decreasing SoH, reflecting the progressive deactivation of silicon. This loss of anode active material (LAAM) in cells cycled at elevated temperatures has been previously documented by Flügel et al. for the same cell type cycled at 0.85C/45 °C and is due to degradation of the Si particles.⁷ It is very probable that the slightly different C-rates of 1C (this work) and 0.85C⁷ lead to similar results.

Figure 2c shows the capacity fade curves for different aging temperatures in the range of −10 °C to 45 °C. The initial aging rates r for the absolute temperatures T were extracted from the initial slopes of Fig. 2c and plotted according to^{12,34}

$$r = A \cdot e^{-E_a/k_B T} \quad [3]$$

with the apparent activation energy E_a , the Boltzmann constant k_B , and the pre-exponential factor A . The Arrhenius plot in Fig. 2d shows two branches, one for temperatures below 10 °C and one above 10 °C. The slope of the low-temperature branch in the

Arrhenius plot indicates that the initial aging rate increases with decreasing temperature. This behavior is typical for Li plating for lab cells^{35,36} and commercial cells^{5,12,36–39} and was also found in simulations.³⁹ The Arrhenius plot in Fig. 2d shows a minimum of the initial aging rate at 10 °C, corresponding to the maximum cycle life and to a transition of the main aging mechanism from Li plating at low temperatures to other dominating side reactions at high temperatures. The high-temperature branch describes the increasing aging rate with increasing temperature and was also observed by others.^{5,12,20,35–41} The occurrence of Li plating in the Arrhenius plot at 1C/0 °C for the cell type under investigation in the present work is consistent with the results of Flügel et al. at 0.85C/0 °C with the same cell type.⁷

The absence of Li plating for cycling at 1C/45 °C is consistent with (i) the slope of the high temperature branch in the Arrhenius plot (Fig. 2d), (ii) with the absence of a shoulder in the voltage curve in Fig. 2a and (iii) with the results by Flügel et al. at 0.85C/45 °C with the same cell type.⁷ Furthermore, the degradation of the Si component at 0.85C/45 °C observed by (iv) Post-Mortem analysis⁷ is consistent with (v) the DVA in Fig. 2b. The shape of the capacity fade curves in Fig. 2c suggests that there are most likely no major changes in the aging mechanism for cyclic aging at 1C/45 °C. Therefore, for the aging at 1C/45 °C mainly investigated in the present work, it can be concluded that LLI and LAAM are most likely the main mechanisms leading to capacity fade until 70% SoH.

ARC analysis.—Cells cycled to different SoH were analyzed by ARC. The resulting self-heating rates (SHR) as a function of temperature are presented in Fig. 3. No discernible differences in SHR are observed in measurements at 100% SoC across varying SoH levels (Fig. 3a). For ARC experiments conducted with

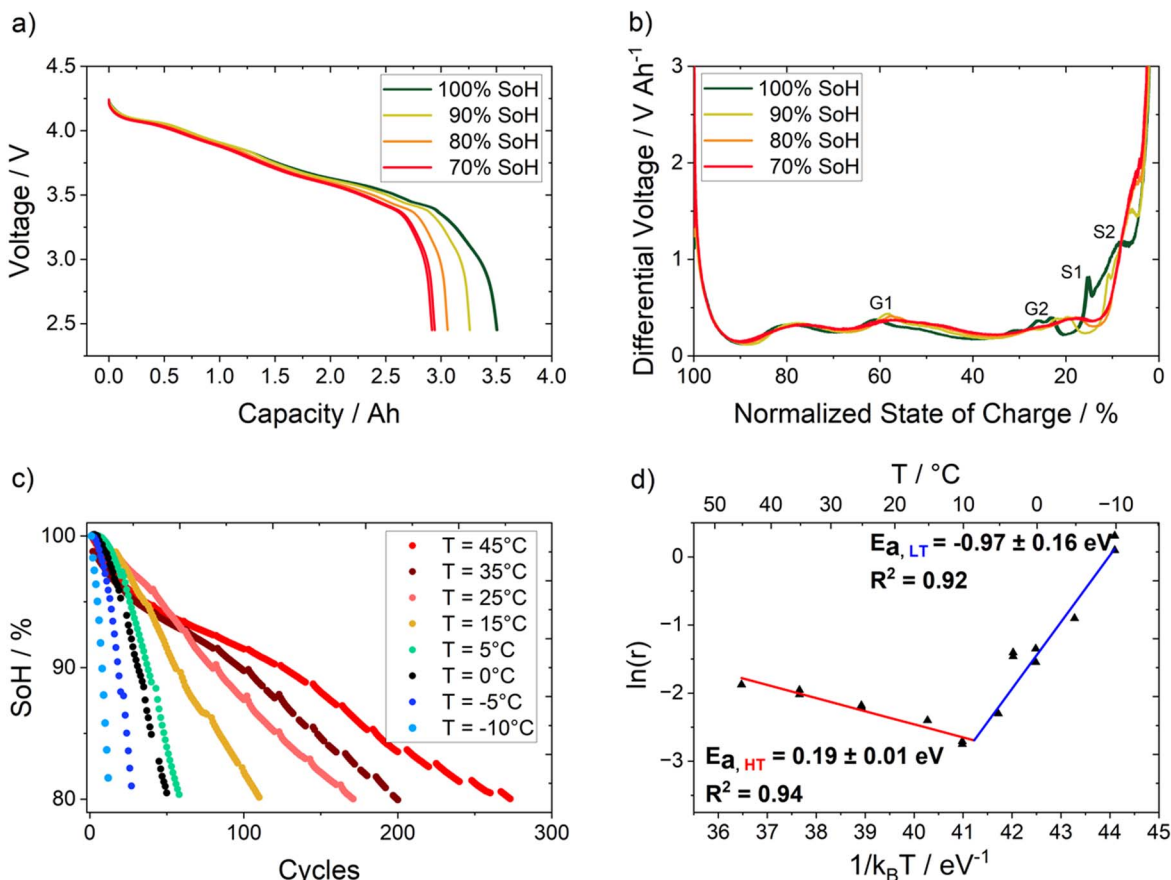


Figure 2. (a) Illustration of qOCV curves at different SoH at 25 °C. (b) Corresponding DVA curves derived from (a). (c) Capacity fade curves for cyclic aging at different temperatures at a rate of 1C. (d) Arrhenius plot derived from the initial aging rates extracted from (c).

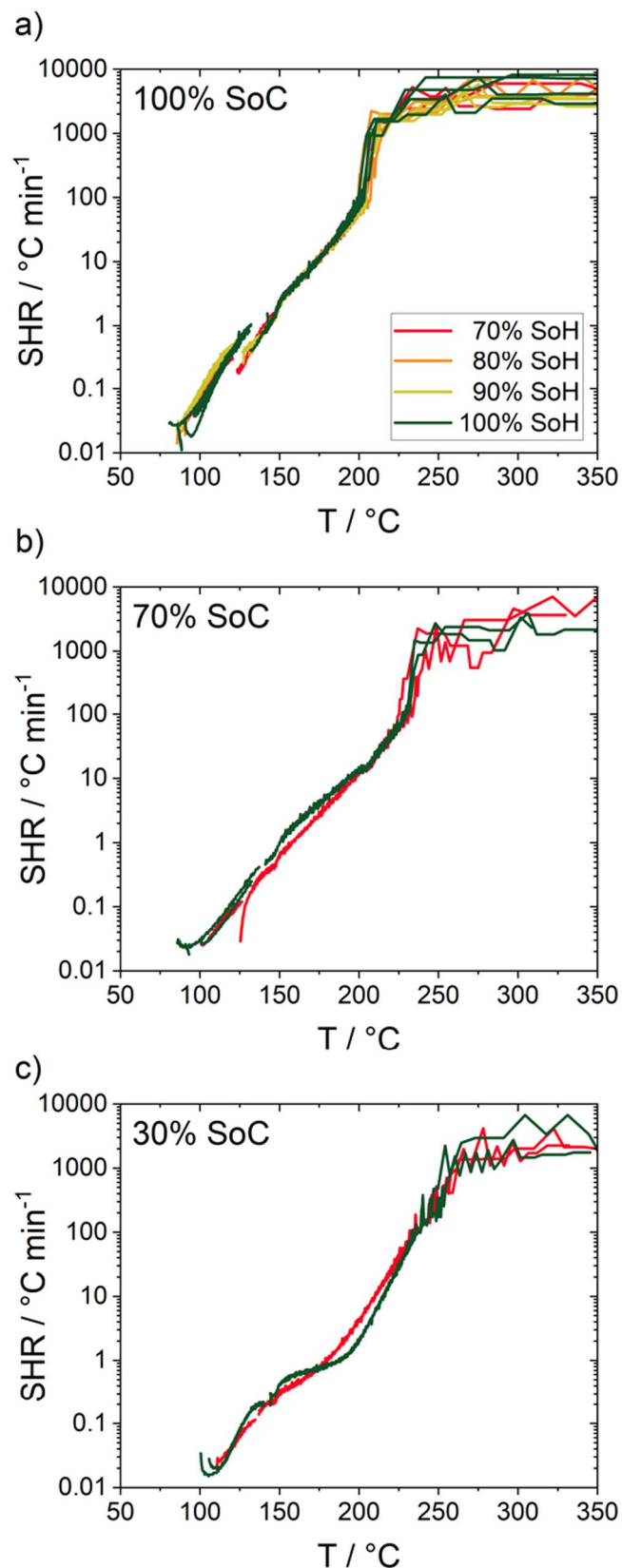


Figure 3. ARC results for (a) 100% SoC, (b) 70% SoC, (c) 30% SoC at different SoH levels.

cells at an SoC of 70% (Fig. 3b) and SoC of 30% (Fig. 3c), minor distinctions between new (SoH = 100%) and aged cells (SoH = 70%) were observed; however, the curve shapes are similar

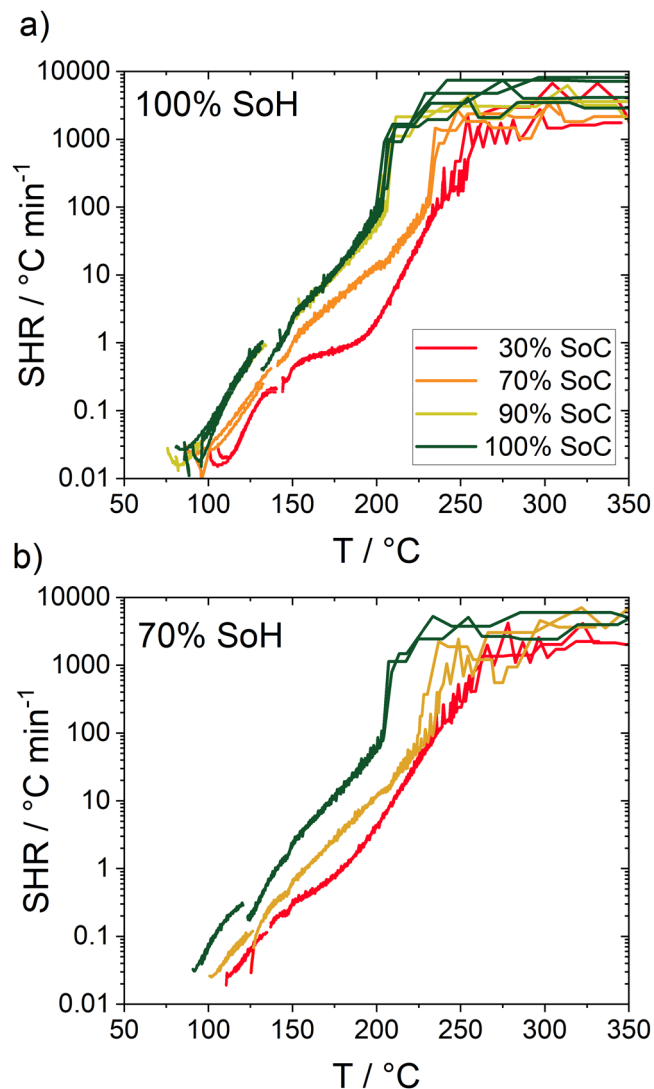


Figure 4. ARC results for (a) 100% SoH, (b) 70% SoH at different SoC levels.

in both cases. These results show that the aging mechanism of SEI growth on the surfaces of graphite particles and degradation of the Si compound (both leading to LLI) and degradation of the Si compound (leading additionally to LAAM) do not influence the safety of the aged cells for ARC experiments conducted at 30%, 70%, and 100% SoC.

When comparing different SoC levels at a fixed SoH, larger differences are observed (Fig. 4). A comparison of the new cells at different SoC is shown in Fig. 4a. The SHR curves are very similar for cells at 90% SoC and 100% SoC. For 70% SoC and 30% SoC, the SHR curves are shifting towards higher temperatures. This shift to higher temperatures with decreasing SoC indicates an increase in safety, which was also observed for other cell types that were not aged.^{15,18,42-44} A comparison of the aged cells with SoH = 70% at different SoC is shown in Fig. 4b. The aged cells show a similar trend with SoC as the new cells.

Figure 5 shows the characteristic temperatures onset of self-heating T_{SH} , venting T_{Vent} , and onset of thermal runaway T_{TR} for different SoH levels as a function of SoC. The T_{SH} increases with decreasing SoC for both new cells and aged cells with SoH = 70% (Fig. 5a). The behavior is consistent with findings from the literature^{15,45-48} and suggests that aged cells offer enhanced thermal stability under the conditions studied (1C/45 $^{\circ}\text{C}$, no Li plating). ARC

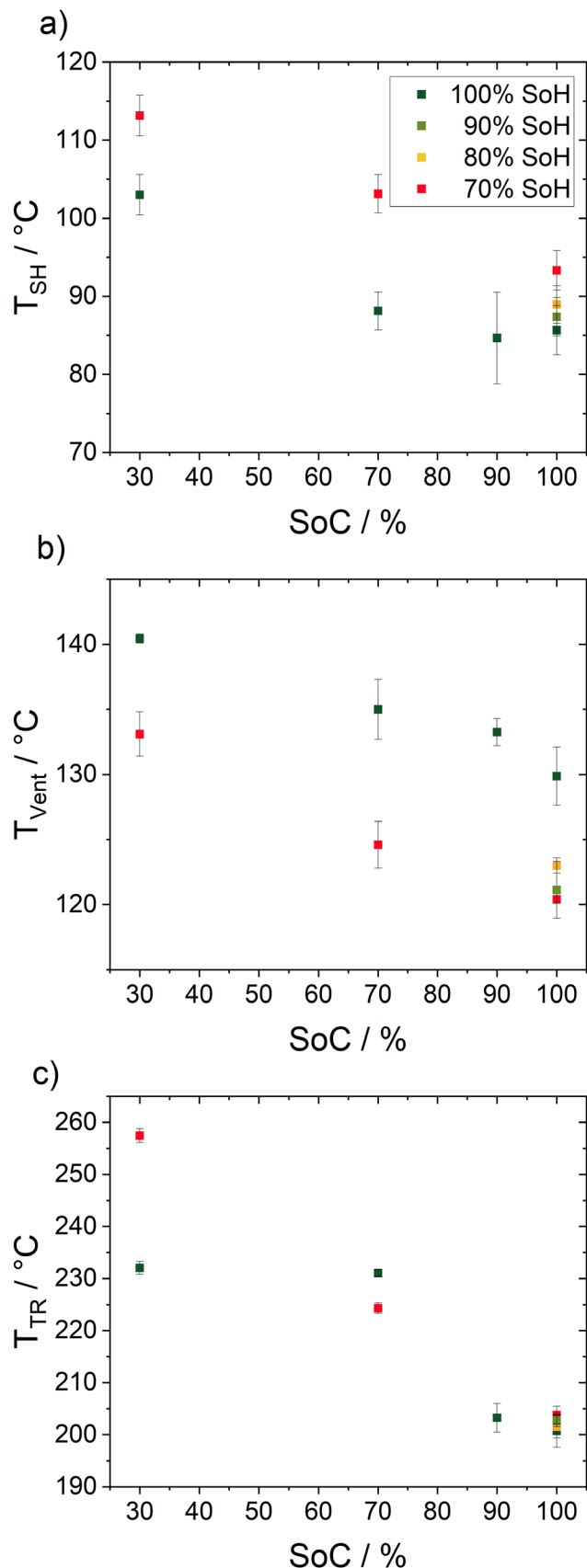


Figure 5. Characteristic temperatures of ARC experiments as a function of SoC and SoH levels.

measurements in Fig. 5a at 100% SoC confirm this trend of increasing T_{SH} with decreasing SoH.

Figure 5b shows a clear trend of decreasing T_{Vent} with higher SoC levels, which aligns well with findings reported in the literature.^{15,44} T_{Vent} is defined as the last measured cell surface temperature before the temperature drop caused by gas release during venting (Joule-Thomson effect). However, while aging enhances cell safety in terms of a delay of T_{SH} for the cells investigated in this study (Fig. 5a), the trend reverses with aging for T_{Vent} . As Fig. 5b shows, T_{Vent} is $\sim 10^\circ C$ lower for SoH = 70% compared with SoH = 100%. This is due to internal pressure build-up, likely from gas generation during degradation.^{44,45,49} ARC measurements at 100% SoC do not show a clear trend of T_{Vent} with SoH. In contrast, cells with a SoH below or equal 90% show similar values for T_{Vent} in the range of 120 to 123 $^\circ C$, whereas the cells at 100% SoC showed a T_{Vent} value of $130 \pm 2^\circ C$.

T_{TR} shows an increase with decreasing SoC (Fig. 5c), which is also consistent with existing studies.^{15,44,46} At 100% SoC, all measurements converge around a similar T_{TR} level of $\sim 200^\circ C$. For ARC measurements at 70% SoC, T_{TR} is also similar for 100% SoH and 70% SoH. These measurements indicate no change in safety level regarding T_{TR} for aging at 1C/45 $^\circ C$. In contrast, T_{TR} is increased for ARC measurements at 30% SoC for the aged cell at 70% SoH ($T_{TR} = 257 \pm 1^\circ C$) compared to $232 \pm 1^\circ C$ for the new cell. This indicates an increase in safety regarding T_{TR} for 30% SoH for the aged cells.

Figure 6 shows the total mass loss after ARC experiments as a function of SoH for different SoC levels. The initial mass of the new cells was measured as $47.7 \text{ g} \pm 0.15 \text{ g}$. The data indicate that cells at 100% SoC and 30% SoC experience the greatest mass loss, whereas those at 70% SoC exhibit comparatively lower mass losses. For new cells of a similar type, the total mass loss at 100% SoC is reported in literature within a range of 63% to 77%.^{15,50,51} These findings align well with the results observed in our study.

Interestingly, cells at 70% SoC exhibit the lowest mass loss for both new cells and aged cells until SoH = 70% compared to those at both high and low SoC. While the cells remained externally intact at high SoC, the degree of damage to the cell housings was most pronounced at lower SoC. This observation is consistent with findings reported in Feinauer et al. for 21700 cells with a similar cell chemistry as in the present work.¹⁵ This weakly indicates that this might be a general trend for cylindrical cells with Ni-rich NMC cathodes and Si/graphite anodes. The behavior is likely attributable to the lower internal gas pressure and energy content at medium SoC levels, which reduces the rate of pulverization and ejection of active material, particularly in contrast to high SoC conditions.¹⁵ Simultaneously, the reactions at 70% SoC occur rapidly enough to avoid lid welding seam failure, which has been observed in cells at 30% SoC following slow heat penetration, which was previously reported for 21700 NMC cells.^{15,52} Nguyen et al. reported a delayed hard internal short circuit and a higher venting temperature in cells with moderate SoC compared to those at high SoC, resulting in more pronounced exothermic reactions occurring at the time of venting, potentially exacerbating thermal events.⁵³ However, due to the higher remaining cell mass at 70% SoC, this condition may present a worst-case scenario for thermal propagation in applications where heat dissipation is limited.

In summary, for ARC tests of new (100% SoH) and 1C/45 $^\circ C$ aged cells (70% SoH), different safety metrics showed different results: (i) The SHR curves were similar for new and aged cells at the same SoC (Fig. 3), (ii) lower SoC lead to decreased SHR levels for both new and aged cells (Fig. 4), (iii) T_{SH} is declining with SoC for new and aged cells (Fig. 5a), (iv) T_{Vent} is also declining with SoC and aged cells exhibit venting at lower temperatures (Fig. 5b), (v) T_{TR} shows an increase with decreasing SoC for both new and aged cells (Fig. 5c), (vi) mass loss for cells at high SoC (100%) and low

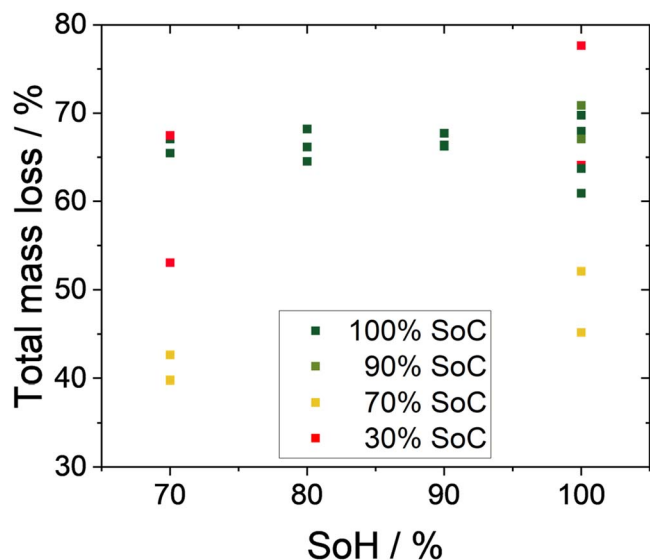


Figure 6. Total mass loss after ARC experiments as a function of SoH and SoC.

SoC (30%) is greater compared to medium SoC (70%) for both new and aged cells (Fig. 6). Overall, the safety level of the aged cells is comparable with that of the new cells for the main aging mechanism of SEI growth and degradation of the Si compound and without Li plating. This is in accordance with ARC experiments^{5,15,22,25,54} and other safety tests of cells without Li plating.⁵⁴ In contrast, cells with Li plating showed a decrease in safety level in ARC experiments^{5,15,21,22,24,25} and other safety tests.²⁴

Impedance analysis.—In the following, the recorded EIS spectra are discussed to investigate impedance changes at the onset of self-heating. Evaluating the self-heating status without the need for T measurement offers advantages in various applications, both for the prevention of rapid aging and for safety evaluation. To address this need, our study proposes a comprehensive self-heating detection logic that incorporates $\text{Re}(Z)_{\text{norm}}$ progression, as well as phase $\phi(Z)_{\text{norm}}$ and Nyquist integral ($I_{N,\text{norm}}$), all of them normalized to T_{start} condition as defined in Eq. 2. This approach ensures robust self-heating behavior monitoring across varying SoC and SoH operational conditions.

In Fig. 7, $\text{Re}(Z)_{\text{norm}}$, $\phi(Z)_{\text{norm}}$ (both at a fixed frequency of 50 mHz) and $I_{N,\text{norm}}$ are shown for new cells as a function of T at high and low SoC. Srinivasan et al. showed that increasing the anode temperature above 75 °C permanently shifts the impedance spectra towards higher $\text{Re}(Z)$ values.¹⁶ Consequently, in a temperature range where polarization effects are no longer dominant in EIS spectra, in general, all frequencies can be used as a T_{SH} detection feature. We note that the point density over temperature varies in Fig. 7 because each measurement prior to ARC self-heating detection was triggered by the ARC wait phase, while measurements after T_{SH} were triggered in equidistant time intervals of 15 min. The measurement was terminated upon reaching the cell voltage limits (2.5 V–4.2 V), resulting in varying end temperatures.

Normalized to T_{start} , new cells exhibit for all SoC levels a U-shaped trend for $\text{Re}(Z)_{\text{norm}}$: All measurements show a significant increase in $\text{Re}(Z)_{\text{norm}}$ beginning at ~ 70 °C (Fig. 7a). The minimum of $\text{Re}(Z)_{\text{norm}}$ decreases with increasing SoC, whereas the slopes of the curves for temperatures above the minimum remain nearly independent of SoC. In general, an increase in impedance at high temperatures has already been reported in the literature.^{16,27,55} Gao et al. observed structural changes in the SEI for cells of another type (NCM622+LMO||graphite) cycled at 80 °C.²⁷ At high temperatures, the SEI has difficulty in maintaining an intact passivation layer, and its continuous decomposition allows the active lithium to be consumed by the reaction with the electrolyte.²⁷ This ongoing SEI

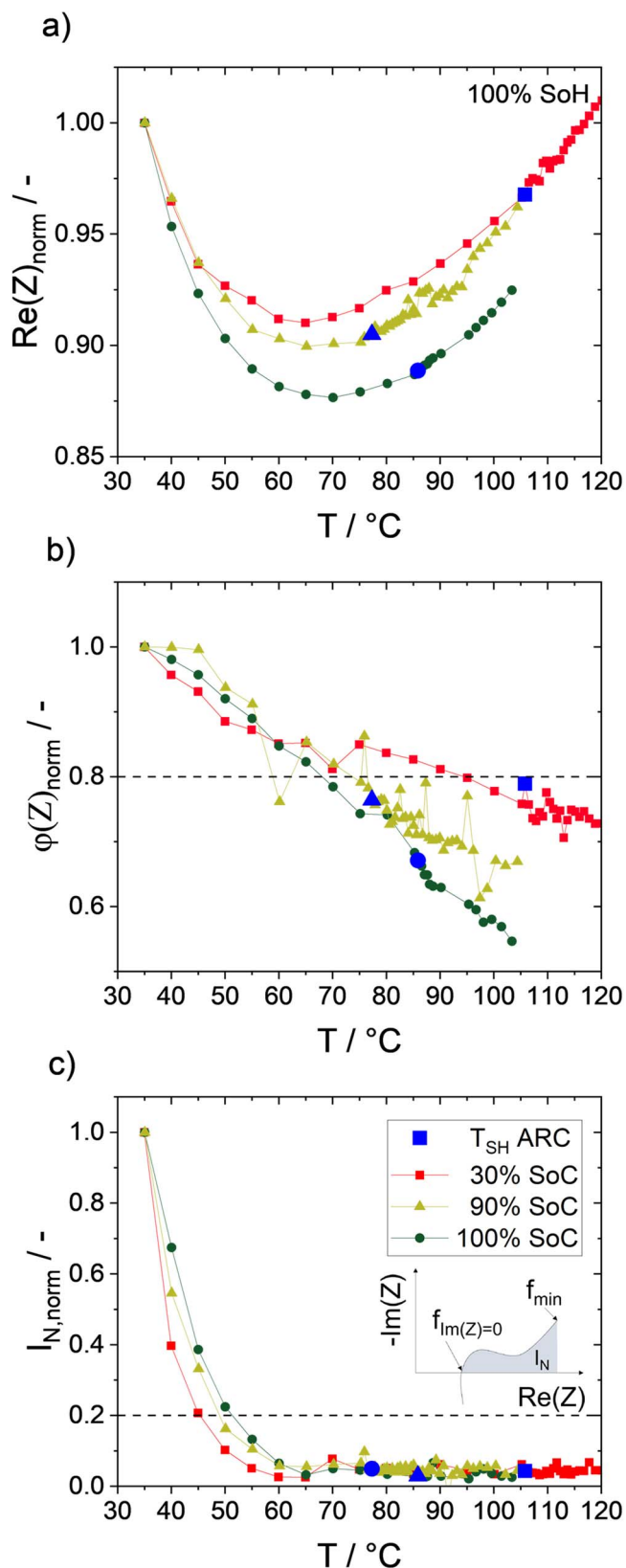


Figure 7. SoC variation impedance measurement inside ARC at 50 mHz for new cells for (a) $\text{Re}(Z)_{\text{norm}}$, (b) $\phi(Z)_{\text{norm}}$, and (c) $I_{N,\text{norm}}$. Onset of self-heating is marked with blue symbols. The inset in (c) shows the graphical interpretation of I_N .

degradation consumes electrolyte, increasing the concentration of lithium salts while reducing ionic conductivity, ultimately leading to higher ohmic resistance.²⁷ It is assumed that the observed increase in

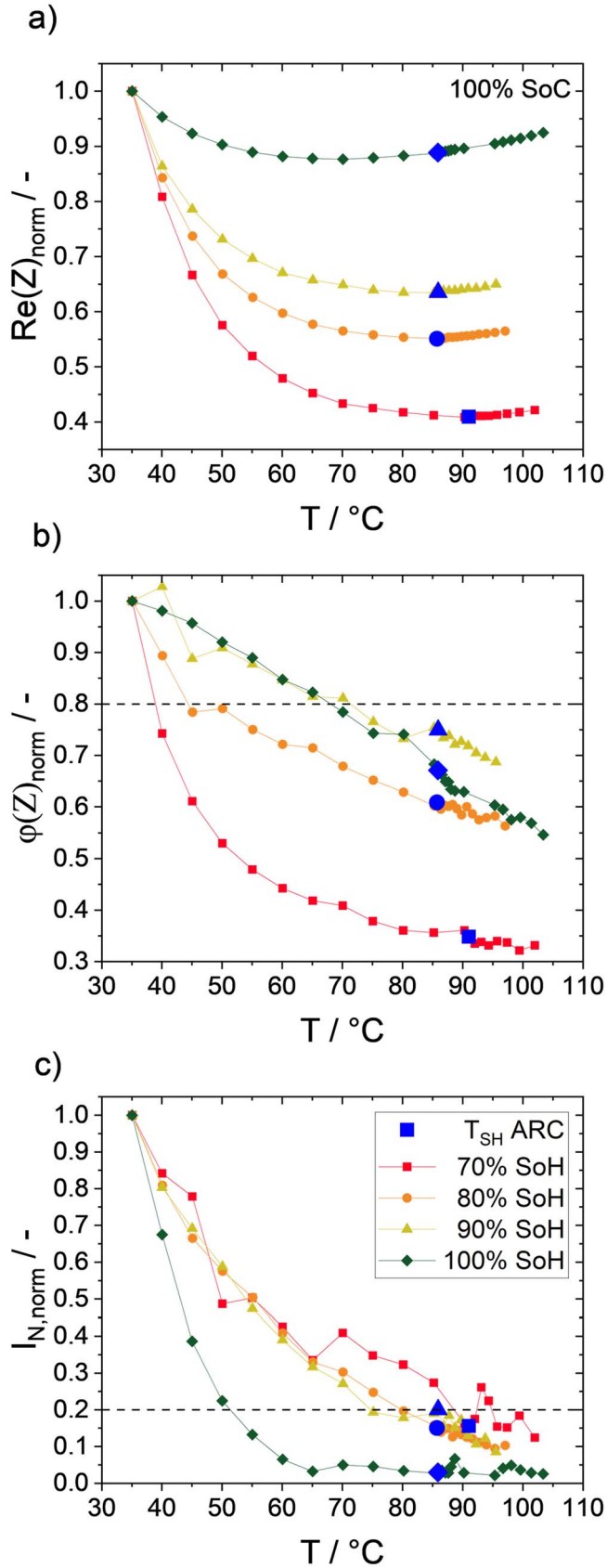


Figure 8. SoH variation impedance measurement inside the ARC chamber at 50 mHz for 100% SoC. Onset of self-heating is marked with blue symbols.

$\text{Re}(Z)_{\text{norm}}$ for new cells in this work is attributable to similar SEI degradation reactions.

Figure 7a demonstrates that for new cells, the minimum of $\text{Re}(Z)_{\text{norm}}$ vs T occurs before the onset of self-heating. The temperature difference between T_{SH} and the minimum of the normalized $\text{Re}(Z)$ progression ($\Delta T = T_{\text{SH}} - T_{\text{min}}$) is 15.9 °C at 100% SoC, 12.1 °C at 90% SoC, and 40.0 °C at 30% SoC. Therefore

$$\frac{d\text{Re}(Z)_{\text{norm}}}{dt} = 0 \quad [4]$$

may serve as an early cell safety evaluation criterion under the condition that T increases monotonically over time. At this point, we note that this criterion alone is insufficient for T_{SH} detection, and additional ones are needed. $\varphi(Z)_{\text{norm}}$ as a second potential T_{SH} indicator is showing an almost linear trend vs T for a wide temperature range (see Fig. 7b) for all SoC levels. A linear $\varphi(Z)_{\text{norm}}$ vs T correlation in a temperature range exceeding regular operation conditions (51 °C–117 °C, prior venting) for fully charged 3 Ah cells of another type is already reported in the literature.²⁶ Figure 7b shows that this trend is also valid for cells at lower SoC. For the cell type investigated, we suggest

$$\varphi(Z)_{\text{norm}} < 0.8 \quad [5]$$

as an additional necessary condition for cell self-heating evaluation. Figure 7c illustrates $I_{N,\text{norm}}$ alongside its graphical interpretation. The integral, calculated numerically using Simpson's method, represents the area under the Nyquist curve within the boundaries where $\text{Im}(Z) < 0$ up to the minimum measured frequency f_{min} . This area includes the polarization regime and diffusion-dominated zone. For all SoC levels, $I_{N,\text{norm}}$ decreases below 0.2 at around 60 °C, which makes it a necessary but not sufficient criterion that is also used herein as a complementary check for T_{SH} detection (Eq. 6).

Figure 8 presents plots of $\text{Re}(Z)_{\text{norm}}$, $\varphi(Z)_{\text{norm}}$, and $I_{N,\text{norm}}$ for different SoH levels at 100% SoC. In all aged cells, the $\text{Re}(Z)_{\text{norm}}$ curves continue to decline due to the high polarization resistance at the beginning of the measurement (Fig. 8a). The slope of the increase after the minimum appears to remain unchanged, suggesting that the same underlying mechanisms are active as in the new cells. The derivative of $\text{Re}(Z)_{\text{norm}}$ in Eq. 4 still appears to be a promising feature for detecting T_{SH} .

Figure 8b shows $\varphi(Z)_{\text{norm}}$ of new and aged cells at different SoH levels. While SoH of 100% and 90% show a similar behavior, aged cells at 80% and 70% exhibit significant differences. The assumption of linearity is therefore no longer valid for aged cells. The observed differences might be attributed to the higher initial polarization resistance at T_{start} for the more aged cells.

In contrast, $I_{N,\text{norm}}$ displays a less steep decrease for aged cells (see Fig. 8c). For the cell type tested, we suggest

$$I_{N,\text{norm}} < 0.2 \quad [6]$$

as a complementary but necessary condition for self-heating evaluation.

For early detection of T_{SH} without temperature measurement, we propose the combination of $\text{Re}(Z)_{\text{norm}}$, $\varphi(Z)_{\text{norm}}$, and $I_{N,\text{norm}}$. Figure 9 shows the result of the proposed T_{SH} detection logic, where conditions from Eq. 4 have to be fulfilled, as well as criteria (5) and (6). For aged cells at 100% SoC, T_{SH} can be predicted without the need for *a priori* knowledge of the cell temperature. The onset of self-heating temperature prediction for new cells at 100% SoC is up to 15 °C lower than observed in ARC measurements, reflecting a conservative bias in estimation. Therefore, our approach seems to be promising for the most critical battery condition, i.e., aged cells in the fully charged state. Limitations of the method are revealed for 30% SoC. Additional experimental data are therefore required in this regime.

ORCID

Thomas Waldmann  <https://orcid.org/0000-0003-3761-1668>

References

- O. Catsaros, (2024), <https://about.bnef.com/insights/commodities/lithium-ion-battery-pack-prices-see-largest-drop-since-2017-falling-to-115-per-kilowatt-hour-bloombergnef/> BloombergNEF.
- X. Feng, M. Ouyang, X. Liu, L. Lu, Y. Xia, and X. He, *Energy Storage Mater.*, **10**, 246 (2018).
- H.-J. Noh, S. Youn, C. S. Yoon, and Y.-K. Sun, *J. Power Sources*, **233**, 121 (2013).
- H. Li, X. Kong, C. Liu, and J. Zhao, *Appl. Therm. Eng.*, **161**, 114144 (2019).
- M. Feinauer, A. A. Abd-El-Latif, P. Sichler, A. Aracil Regalado, M. Wohlfahrt-Mehrens, and T. Waldmann, *J. Power Sources*, **570**, 233046 (2023).
- T. M. M. Heenan, A. Jnawali, M. D. R. Kok, T. G. Tranter, C. Tan, A. Dimitrijevic, R. Jervis, D. J. L. Brett, and P. R. Shearing, *J. Electrochem. Soc.*, **167**, 140530 (2020).
- M. Flügel, K. Richter, M. Wohlfahrt-Mehrens, and T. Waldmann, *J. Electrochem. Soc.*, **169**, 50533 (2022).
- M. Schindler, J. Sturm, S. Ludwig, A. Durdal, and A. Jossen, *J. Electrochem. Soc.*, **168**, 60522 (2021).
- X. Li, A. M. Colclasure, D. P. Finegan, D. Ren, Y. Shi, X. Feng, L. Cao, Y. Yang, and K. Smith, *Electrochim. Acta*, **297**, 1109 (2019).
- M. Broussely, S. Herreyre, P. Biensan, P. Kaszteljna, K. Nechev, and R. Staniewicz, *J. Power Sources*, **97-98**, 13 (2001).
- N. Ghanbari, T. Waldmann, M. Kasper, P. Axmann, and M. Wohlfahrt-Mehrens, *J. Phys. Chem. C*, **120**, 22225 (2016).
- T. Waldmann, M. Wilka, M. Kasper, M. Fleischhammer, and M. Wohlfahrt-Mehrens, *J. Power Sources*, **262**, 129 (2014).
- J. C. Burns, D. A. Stevens, and J. R. Dahn, *J. Electrochem. Soc.*, **162**, A959 (2015).
- T. Waldmann, B.-I. Hogg, and M. Wohlfahrt-Mehrens, *J. Power Sources*, **384**, 107 (2018).
- M. Feinauer, A. A. Abd-El-Latif, P. Sichler, M. Wohlfahrt-Mehrens, M. Hölzle, and T. Waldmann, *J. Electrochem. Soc.*, **171**, 110524 (2024).
- R. Srinivasan, P. A. Demirev, and B. G. Carkhuff, *J. Electrochem. Soc.*, **169**, 20522 (2022).
- C. Uhlmann, J. Illig, M. Ender, R. Schuster, and E. Ivers-Tiffée, *J. Power Sources*, **279**, 428 (2015).
- B. Mao, P. Huang, H. Chen, Q. Wang, and J. Sun, *Int. J. Heat Mass Transfer*, **149**, 119178 (2020).
- M. N. Richard and J. R. Dahn, *J. Electrochem. Soc.*, **146**, 2068 (1999).
- M. Fleischhammer, T. Waldmann, G. Bisle, B.-I. Hogg, and M. Wohlfahrt-Mehrens, *J. Power Sources*, **274**, 432 (2015).
- T. Waldmann and M. Wohlfahrt-Mehrens, *Electrochim. Acta*, **230**, 454 (2017).
- T. Waldmann, J. B. Quinn, K. Richter, M. Kasper, A. Trost, A. Klein, and M. Wohlfahrt-Mehrens, *J. Electrochem. Soc.*, **164**, A3154 (2017).
- M. Feinauer, M. Hölzle, and T. Waldmann, *Electrochem. Soc. Interface*, **33**, 51 (2024).
- G. G. Gerosa, M. Feinauer, C. Hogrefe, S. Häfele, K. Bischof, M. Wörz, O. Böse, M. Wohlfahrt-Mehrens, M. Hölzle, and T. Waldmann, *J. Electrochem. Soc.*, **172**, 30502 (2025).
- Y. Preger, L. Torres-Castro, T. Rauhala, and J. Jeevarajan, *J. Electrochem. Soc.*, **169**, 30507 (2022).
- R. Srinivasan, P. A. Demirev, and B. G. Carkhuff, *J. Power Sources*, **405**, 30 (2018).
- T. Gao, J. Bai, D. Ouyang, Z. Wang, W. Bai, N. Mao, and Y. Zhu, *Renewable Energy*, **203**, 592 (2023).
- M. Steinhauer, S. Risse, N. Wagner, and K. A. Friedrich, *Electrochim. Acta*, **228**, 652 (2017).
- R. Srinivasan, B. G. Carkhuff, M. H. Butler, and A. C. Baisden, *Electrochim. Acta*, **56**, 6198 (2011).
- J. B. Quinn, T. Waldmann, K. Richter, M. Kasper, and M. Wohlfahrt-Mehrens, *J. Electrochem. Soc.*, **165**, A3284 (2018).
- B. Lei, W. Zhao, C. Ziebert, N. Uhlmann, M. Rohde, and H. J. Seifert, *10.20944/preprints201702.0033.v1* (2017).
- C. von Lüders, V. Zinth, S. V. Erhard, P. J. Osswald, M. Hofmann, R. Gilles, and A. Jossen, *J. Power Sources*, **342**, 17 (2017).
- C. Hogrefe, S. Hein, T. Waldmann, T. Danner, K. Richter, A. Latz, and M. Wohlfahrt-Mehrens, *J. Electrochem. Soc.*, **167**, 140546 (2020).
- P. W. Atkins, *Physical Chemistry* (Oxford University Press, Oxford; New York) (1990).
- M. Feinauer, M. Wohlfahrt-Mehrens, M. Hölzle, and T. Waldmann, *J. Electrochem. Soc.*, **171**, 110506 (2024).
- M. Bozorgchenani, G. Kucinskis, M. Wohlfahrt-Mehrens, and T. Waldmann, *J. Electrochem. Soc.*, **169**, 30509 (2022).
- G. Kucinskis, M. Bozorgchenani, M. Feinauer, M. Kasper, M. Wohlfahrt-Mehrens, and T. Waldmann, *J. Power Sources*, **549**, 232129 (2022).
- M. Feinauer, M. Wohlfahrt-Mehrens, M. Hölzle, and T. Waldmann, *J. Power Sources*, **594**, 233948 (2024).
- X.-G. Yang and C.-Y. Wang, *J. Power Sources*, **402**, 489 (2018).
- B. Y. Liaw, E. P. Roth, R. G. Jungst, G. Nagasubramanian, H. L. Case, and D. H. Doughty, *J. Power Sources*, **119-121**, 874 (2003).
- S. Käbitz, J. B. Gerschler, M. Ecker, Y. Yurdağel, B. Emmertmacher, D. André, T. Mitsch, and D. U. Sauer, *J. Power Sources*, **239**, 572 (2013).

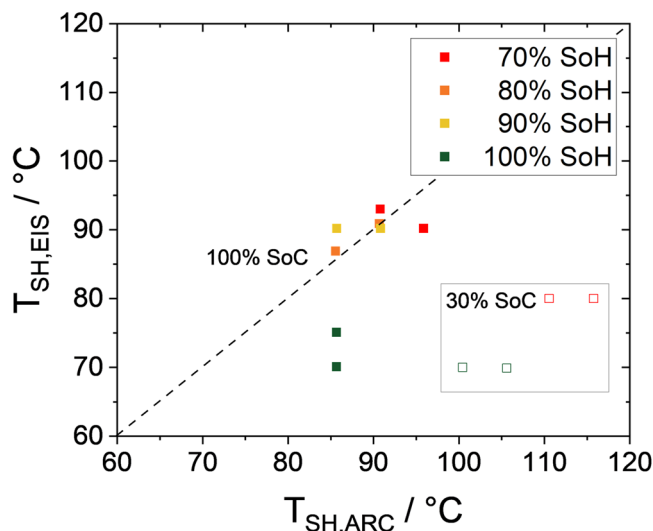


Figure 9. T_{SH} determined using impedance detection logic vs T_{SH} determined in ARC measurements.

Conclusions

In this study, with 3.5 Ah commercial cylindrical Li-ion cells containing a Si/C anode and a Ni-rich NMC cathode, the safety behavior for different SoH (100%, 90%, 80%, 70%) and SoC (100%, 90%, 70%, 30%) was investigated by ARC.

For the investigated cell type, no evidence of Li plating was observed in electrochemical measurements for cells aged at 45°C at a rate of 1C. LLI and LAAM are most likely the main mechanisms leading to capacity fade until 70% SoH. This is consistent (i) with the slope of the high temperature branch in the Arrhenius plot, (ii) with the absence of a shoulder in the discharge voltage curve, and (iii) with the vanishing of the Si peaks in DVA.

The aging mechanism of SEI growth on the surfaces of graphite particles and degradation of the Si compound (both leading to LLI) and degradation of the Si compound (leading additionally to LAAM) do not significantly influence the safety of the aged cells in ARC experiments conducted at 30%, 70%, and 100% SoC. Both, onset temperature of self-heating T_{SH} and venting temperature T_{Vent} exhibit linear trends with respect to the SoC across all SoH conditions. Over the course of the cell's lifetime, T_{SH} increases, while T_{Vent} decreases by up to 10 °C. The mass loss is lowest at intermediate SoC levels. Additionally, there is a slight trend toward lower total mass loss in aged cells, which may indicate a reduction in energy release due to degradation-related capacity.

Overall, the results indicate that the investigated cells do not exhibit a decline in safety over their lifetime. Consequently, it can be concluded that for the investigated cell type, new cells represent the “worst-case” scenario for battery safety performance when compared to high-temperature-aged cells. This finding suggests that the evaluation of cell safety for second-life applications might be effectively conducted using new cells if lithium depositions are absent.

Finally, a combination of ARC and EIS (ARC-EIS) shows that T_{SH} correlates with features from EIS measurements. Thus, impedance-based methods, specifically the evaluation of the curve progression of $\text{Re}(Z)_{\text{norm}}$ in combination with $\phi(Z)_{\text{norm}}$ and $I_{N,\text{norm}}$ evaluation, seem to be promising for early detecting the onset of self-heating in cells at high SoC. We note that this method still has limitations, e.g., at low SoC. Further work in this direction is needed, e.g., on different aging mechanisms and cell chemistries.

Acknowledgments

All investigations in this work were carried out at ZSW Ulm. The authors would like to thank the ZSW members M. Feinauer, A. A. Abd-El-Latif, and P. Sichler for their support.

42. A. Kvasha, C. Gutiérrez, U. Osa, I. de Meatza, J. A. Blazquez, H. Macicior, and I. Urdampilleta, *Energy*, **159**, 547 (2018).
43. W.-C. Chen, J.-D. Li, C.-M. Shu, and Y.-W. Wang, *J. Therm. Anal. Calorim.*, **121**, 525 (2015).
44. C. Zhao, J. Sun, and Q. Wang, *Journal of Energy Storage*, **28**, 101232 (2020).
45. Y. Li, X. Feng, D. Ren, M. Ouyang, L. Lu, and X. Han, *ACS Appl. Mater. Interfaces*, **11**, 46839 (2019).
46. X. He, Z. Hu, F. Restuccia, J. Fang, and G. Rein, *Appl. Therm. Eng.*, **212**, 118621 (2022).
47. J. Lamb, L. Torres-Castro, J. C. Hewson, R. C. Shurtz, and Y. Preger, *J. Electrochem. Soc.*, **168**, 60516 (2021).
48. O. Willstrand, M. Pushp, P. Andersson, and D. Brandell, *Journal of Energy Storage*, **68**, 107785 (2023).
49. A. A. Abd-El-Latif, P. Sichler, M. Kasper, T. Waldmann, and M. Wohlfahrt-Mehrens, *Batteries & Supercaps*, **4**, 1135 (2021).
50. Y. Fedoryshyna, S. Schaeffler, J. Soellner, E. I. Gillich, and A. Jossen, *J. Power Sources*, **615**, 235064 (2024).
51. W. Q. Walker, J. J. Darst, D. P. Finegan, G. A. Bayles, K. L. Johnson, E. C. Darcy, and S. L. Rickman, *J. Power Sources*, **415**, 207 (2019).
52. S. Ohneseit, P. Finster, C. Floras, N. Lubenau, N. Uhlmann, H. J. Seifert, and C. Ziebert, *Batteries*, **9**, 237 (2023).
53. T. T. D. Nguyen, S. Abada, A. Lecocq, J. Bernard, M. Petit, G. Marlair, S. Grugeon, and S. Laruelle, *World Electric Vehicle Journal*, **10**, 79 (2019).
54. Y. Preger et al., *J. Electrochem. Soc.*, **172**, 080503 (2025).
55. N. Orazov, "Methode Zur Zustandsbewertung Thermisch Beschädigter Lithium-Ionen-Zellen." *Dissertation*, Technische Universität Clausthal (2024), <https://doi.org/10.21268/20240429-0>.